Computation of electromagnetic forces in the windings of amorphous core transformers

BAO DOAN THANH [✉], DOAN DUC TUNG, TUAN-HO LE

Faculty of Engineering and Technology, Quy Nhon University
Binh Dinh province, Vietnam
e-mail: {✉doanthanhbao/doanductung/tuanhole}@qnu.edu.vn

Abstract: Electromagnetic forces generated by the short circuit current and leakage flux in low- and high-voltage windings of distribution transformers as well as amorphous core transformers will cause the translation, destruction, and explosion of the windings. Thus, the investigation of these forces plays a significant role for researchers and manufacturers. Many authors have recently used the finite element method to analyze electromagnetic forces. In this paper, an analytic model is first developed for magnetic vector potential formulations to compute the electromagnetic forces (i.e., axial and radial forces) acting on the low- and high-voltage windings of an amorphous core transformer. The finite element technique is then presented to validate the results obtained from the analytical model. The developed model is applied to an actual problem.

Key words: amorphous transformer, electromagnetic force, leakage flux, magnetic vector potential formulation, short-circuit current

1. Introduction

Nowadays, amorphous transformers have been widely utilized in power systems due to no-load losses being less than those of silicon steel core transformers by a rate of 60%–70% [1–4]. This leads to the reduction of total losses of the power system. For the mode of load and no-load operations, the main parameters of transformers must be concerned such as efficiency, loss, temperature rise, and core weight [5–8]. As a sudden short-circuit in the low-voltage winding of the transformer or a short-circuit between connected turns occurs, the magnetic flux distribution in the magnetic circuit is small, but the leakage/fringing flux in the air gap is very large. The interaction of the leakage flux and the short-circuit current in the windings will produce excessive

electromagnetic forces (EMF), which cause the translation, destruction, or explosion of the windings [5, 6, 9–12].

A ribbon of steel is wound to form the core of an amorphous transformer. While the steel foil of the amorphous transformer is arranged in the z-direction, the one of silicon steel core transformer is established in the horizontal x. Therefore, the cross-section of a pillar of the magnetic circuit of the amorphous transformer is rectangular. The cross-section of a pillar of the magnetic circuit of the silicon steel core transformer is rectangular. Consequently, the distribution of the electric field and the distribution of forces on the windings of the transformer are uneven. In addition, the insulation strength and winding strength of the amorphous transformer will be worse than those of the silicon steel core transformer [13, 14].

It should be noted that the winding faults account for a high percentage of all transformer faults, with a rate of 33%. Most of these winding faults are short-circuit between the turns of low-voltage (LV) or high-voltage (HV) windings, between layers of windings, or between phases in the same winding, etc. These faults will make a very high EMF or mechanical force in the windings [15]. This EMF is split into two components, i.e., axial force (F_x) and radial force (F_y), where F_x is generated by the interaction of the current in the winding and the axial leakage magnetic field (B_y) being perpendicular to the winding axis, and F_y generated by the interaction of the current in the winding and the horizontal leakage magnetic field (B_x) being parallel to the winding axis [3, 5, 14, 15].

Many researchers have recently used the finite element method (FEM) to analyze and compute the leakage magnetic field and EMFs for transformers. In Reference [14], the authors examined the calculated magnetic field distribution in the amorphous core transformers under the short-circuit condition including the flux by the voltage supplying. The magnetically asymmetrical transformer was also compared with the symmetrical one obtained from the FEM. In Reference [16], the FEM was presented to analyze the mechanical stresses in LV and HV windings of a power transformer of 20 MVA–132/11.5 kV. In this study, a 2D model was considered with the leakage flux and EMFs obtained from both the FEM and the analytical method. Authors also investigated the effects of asymmetrical short-circuit currents and forces in various parts of LV and HV windings. In Reference [17], the FEM was applied to analyze the influence of the short-circuit current on a three-phase transformer of 70 MVA–220/3.6/6.9 kV. A 2D asymmetric field-circuit-coupled nonlinear transient finite-element model was developed to investigate the transient axial and radial forces in the windings. In Reference [20], the short-circuit withstanding ability of a shell-form power transformer with amorphous alloy cores of 800 kVA-10/0.4 kV was proposed. In this study, the stress and strain of the end covers and the winding clamps were computed. Based on the obtained results, a new structure measurement of pulling screws to compress the clamps and the coils was suggested for researchers and manufacturers. In Reference [22], a short-circuit withstand test of Metglas 2605SA1 based on the amorphous distribution transformers was pointed out. In this approach, the electro-dynamic forces between two rectangular windings were evaluated. However, the distribution of the leakage magnetic field and the EMFs (F_x and F_y) in the windings were not considered. In References [3, 10, 12, 18–21], the distribution of leakage magnetic field, leakage reactance, and EMFs in the LV and HV windings under short-circuit conditions were considered via the 2D-FEM. The leakage magnetic field density and average EMFs obtained from the FEM were compared with the obtained results of the analytical method.

As the above analyzed, most of the studies focus on investigating and computing the EMFs in the LV and HV windings under short-circuit conditions. However, the comprehensive analytic model to calculate these EMFs has been not presented in previous studies yet. In addition, the comparison of results between the analytic method and FEM has been not also mentioned so far.

In this paper, a mathematical model for leakage magnetic fields and EMFs in amorphous transformer windings is first developed with the magnetic vector potential formulations to calculate the leakage magnetic fields and EMFs in the LV and HV windings. Then, the FEM is also extended to prove the validation of the developed model. The development of two proposed methods is validated on a three-phase amorphous transformer winding of 160 kVA–22/0.4 kV under three-phase short-circuit conditions. The process for computing the EMFs in the amorphous transformer windings is pointed out in Fig. 1.
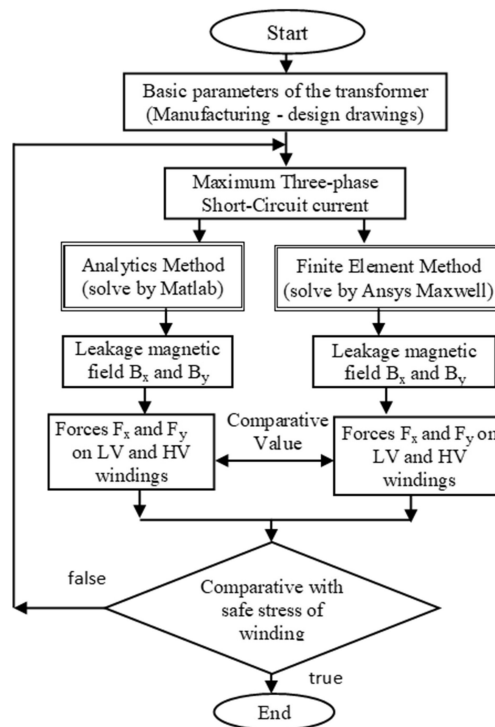

Fig. 1. Process of computation of EMFs in the amorphous transformer windings

2. Development of a mathematical model of magnetic vector potential A

2.1. Analytical modeling of magnetic vector potential A

Maxwell's equations considered in the frequency domain and behavior laws are written in Euclidean space $\mathbb{R}^3$ [1, 2, 10]:

$$\text{rot}\,\boldsymbol{H} = \boldsymbol{J}, \tag{1}$$

$$\text{rot}\,\boldsymbol{E} = -j\omega\boldsymbol{B}, \tag{2}$$

$$\text{div}\,\boldsymbol{B} = 0, \tag{3}$$

$$\boldsymbol{B} = \mu\boldsymbol{H}, \tag{4}$$

$$\boldsymbol{J} = \sigma\boldsymbol{E}, \tag{5}$$

where: $\boldsymbol{H}$ is the magnetic field (A/m), $\boldsymbol{B}$ is the magnetic flux density (T), $\boldsymbol{E}$ is the electric field (V/m), $\boldsymbol{J}_s$ is the current density (A/m^2), μ and σ are, respectively, the relative permeability and electric conductivity (S/m).

From Eq. (3), the magnetic vector potential ($\boldsymbol{A}$) can be defined as:

$$\boldsymbol{B} = \text{rot}\,\boldsymbol{A} \quad \text{or,} \quad \boldsymbol{B} = \nabla \times \boldsymbol{A}. \tag{6}$$

Hence,

$$\text{div}\,(\text{rot}\,\boldsymbol{A}) = 0. \tag{7}$$

By substituting Eq. (6) and Eq. (7) into Eq. (1), Laplace–Poisson's equation for $\boldsymbol{A}$ can be represented as [8, 11]:

$$\nabla^2\boldsymbol{A} = -\mu\boldsymbol{J}. \tag{8}$$

In three-dimensional Descartes coordinates, it can be written as:

$$\frac{\partial^2 \boldsymbol{A}}{\partial x^2} + \frac{\partial^2 \boldsymbol{A}}{\partial y^2} + \frac{\partial^2 \boldsymbol{A}}{\partial z^2} = -\mu\boldsymbol{J}. \tag{9}$$

In this paper, the term $\boldsymbol{A}$ is investigated in the window area of the transformer. For that, in the 2D Descartes coordinates (xy), one has

$$\begin{cases} \boldsymbol{B}_z = 0 \\ \dfrac{\partial \boldsymbol{A}}{\partial z} = 0 \end{cases}. \tag{10}$$

Equation (9) can be rewritten as:

$$\frac{\partial^2 \boldsymbol{A}}{\partial x^2} + \frac{\partial^2 \boldsymbol{A}}{\partial y^2} = -\mu\boldsymbol{J}. \tag{11}$$

From Eq. (6) and Eq. (10), it can be derived

$$\begin{cases} \boldsymbol{B}_x = \dfrac{\partial \boldsymbol{A}}{\partial y} \\ \boldsymbol{B}_y = -\dfrac{\partial \boldsymbol{A}}{\partial x} \\ \boldsymbol{B}_z = 0 \end{cases}. \tag{12}$$

The dimensions of a window of an amorphous transformer are given in Fig. 2.

By neglecting the magnetization current, the total magneto-motive forces (MMFs) can be expressed as:

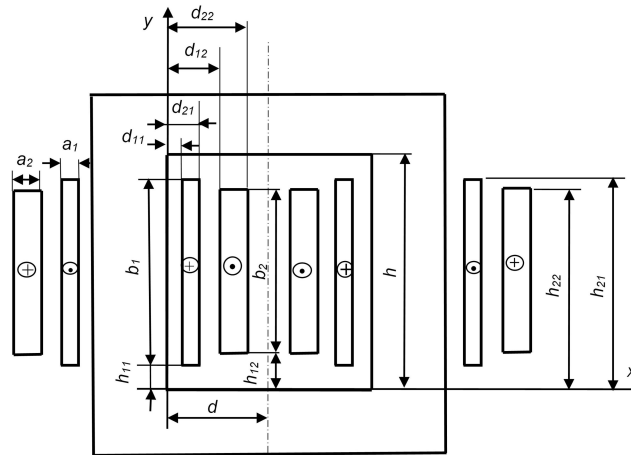$$\sum_{s=1}^{g} W_s i_s = 0, \tag{13}$$

Fig. 2. Dimensions of the window of an amorphous transformer

where: g is the total number of windings in the transformer, W_s is the number of s-th winding and i_s is the electric current in the s-th winding. If the insulation between turns in the coil is thin, the total cross-section of the s-th winding approximately will be $a_s b_s$. By neglecting the effect of eddy current, the current density can be represented as follows:

$$J_s = \pm \frac{W_s i_s}{a_s b_s}, \tag{14}$$

where the "+" and "–" signs show the reverse directions of the currents in the HV and LV windings.

Equation (14) can be rewritten as follows:

$$\sum_{s=1}^{g} J_s a_s b_s = 0. \tag{15}$$

It should be noted that the magnetic permeability of the core material is much greater than the magnetic permeability of the air. Hence, at the contact layer between two surfaces, the tangential component of the magnetic field will be eliminated. Therefore, boundary conditions (BCs) are defined as:

$$\begin{cases} \boldsymbol{B}_{x(y=0,h)} = 0 \\ \boldsymbol{B}_{y(x=0,d)} = 0 \end{cases}. \tag{16}$$

As shown in Fig. 2, at the symmetrical axis (i.e., $x = d$), the component of the magnetic field can be calculated as:

$$\boldsymbol{B}_{y(x=d)} = \left(-\frac{\partial A}{\partial x} \right)_{x=d} = 0. \tag{17}$$

The components of the magnetic field in the x and y axes at the boundaries of the window can be defined as:

$$\boldsymbol{B}_x = \left(\frac{\partial A}{\partial y} \right)_{y=0} = \left(\frac{\partial A}{\partial y} \right)_{y=h} = 0, \tag{18}$$

$$\boldsymbol{B}_y = \left(\frac{\partial \boldsymbol{A}}{\partial x}\right)_{x=0} = \left(\frac{\partial \boldsymbol{A}}{\partial x}\right)_{x=h} = 0. \tag{19}$$

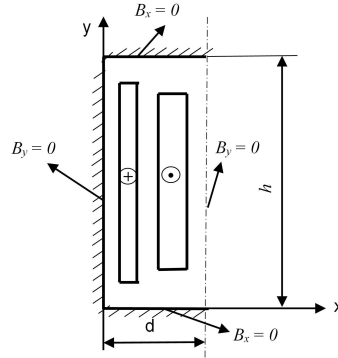The magnetic field components at the boundaries of the window of a transformer can be presented in Fig. 3.

Fig. 3. Magnetic field components at the boundaries in the *x* and *y* axes

In order to solve Eq. (9), it is supposed that the general solution of $\boldsymbol{A}$ in the form of a harmonic series is

$$\boldsymbol{A}(x, y) = \sum_j \sum_k A_{j,k} \cos(m_j x) \cdot \cos(n_k y), \tag{20}$$

where $A_{j,k}$ is the constant of integration calculation. m and n are the phase angle (rad).

In order to satisfy Eq. (18) with $y = 0$ and Eq. (19) with $x = 0$, the BCs are defined as:

$$\sin(m_j d) = 0 \quad \rightarrow \quad m_j = (j-1)\frac{\pi}{d}, \tag{21}$$

$$\sin(n_k h) = 0 \quad \rightarrow \quad n_k = (k-1)\frac{\pi}{h}, \tag{22}$$

where j and k are the integers.

By taking the second derivative of Eq. (20), the magnetic potential equation in the *s*-th winding is:

$$\sum_j \sum_k \left(m_j^2 + n_k^2\right) A_{j,k} \cos(m_j x) \cdot \cos(n_k y) = \mu_0 J_s . \tag{23}$$

By taking the integration of Eq. (23), from 0 to d following the *x*-axis and from 0 to h following the *y*-axis, as presented in Fig. 3, it can be considered with two different cases:

+ Case 1: For two windings, one gets:

$$\left(m_j^2 + n_k^2\right) A_{j,k} \int_0^d \cos^2\left(m_j x\right) \mathrm{d}x \int_0^h \cos^2\left(n_k y\right) \mathrm{d}y$$

$$= \mu_0 \left(J_1 \int_{d_{11}}^{d_{21}} \cos(m_j x)\,\mathrm{d}x \int_{h_{11}}^{h_{21}} \cos(n_k y)\,\mathrm{d}y + J_2 \int_{d_{12}}^{d_{22}} \cos(m_j x)\,\mathrm{d}x \int_{h_{12}}^{h_{22}} \cos(n_k y)\,\mathrm{d}y\right). \tag{24}$$

+ Case 2: For many windings, such as g windings, one can be defined as:

$$\left(m_j^2 + n_k^2\right) A_{j,k} \int_0^d \cos^2\left(m_j x\right) \, \mathrm{d}x \int_0^h \cos^2\left(n_k y\right) \, \mathrm{d}y$$

$$= \sum_{s=1}^g \mu_0 J_s \left(\int_{d_{1s}}^{d_{2s}} \cos(m_j x) \, \mathrm{d}x \int_{h_{1s}}^{h_{2s}} \cos(n_k y) \, \mathrm{d}y \right). \tag{25}$$

For $j = 1$, $k \neq 1$, $m_j = 0$, $n_k = (k-1)\dfrac{\pi}{h}$, based on Eq. (25), the constant of integration can be derived as:

$$A_{1,k} = \frac{2\mu_0}{n_k^3 dh} \sum_{s=1}^g J_s a_s \left[\sin(n_k h_{2s}) - \sin(n_k h_{1s})\right], \tag{26}$$

for $j \neq 1$, $k = 1$, $m_j = 0$, $n_k = 0$, based on Eq. (25), the constant of integration can be derived as:

$$A_{j,1} = \frac{2\mu_0}{m_k^3 dh} \sum_{s=1}^g J_s b_s \left[\sin(m_j d_{2s}) - \sin(m_j d_{1s})\right]. \tag{27}$$

The constant of integration can be generally illustrated as:

$$A_{j,k} = \frac{4\mu_0}{dh} \frac{1}{m_j n_k \left(m_j^2 + n_k^2\right)} \sum_{s=1}^g J_s \left[\sin(m_j d_{2s}) - \sin(m_j d_{1s})\right] \left[\sin(n_k h_{2s}) - \sin(n_k h_{1s})\right], \tag{28}$$

for $j = k = 1$ and $m_1 = n_1 = 0$, the harmonic sequence is constant.

2.2. Computation of electromagnetic forces in the windings

Based on the magnetic vector potential, according to Lorentz's law, F_x per unit length of the s-th winding in the x-axis can be defined as [1, 2]:

$$F_{x,s} = \int_{d_{1s}}^{d_{2s}} \int_{h_{1s}}^{h_{2s}} J_s B_y \, \mathrm{d}x \, \mathrm{d}y = -J_s \int_{d_{1s}}^{d_{2s}} \int_{h_{1s}}^{h_{2s}} \frac{\partial A}{\partial x} \, \mathrm{d}x \, \mathrm{d}y. \tag{29}$$

From Eq. (28), Eq. (29) can be written as:

$$F_{x,s} = J_s \sum_{j=1}^\infty \sum_{k=1}^\infty \frac{A_{j,k}}{n_k} \left[\sin(n_k h_{2s}) - \sin(n_k h_{1s})\right] \left[\cos(m_j d_{2s}) - \cos(m_j d_{1s})\right]. \tag{30}$$

Similarly, F_y per unit length of the s-th winding in the y-axis can be defined as:

$$F_{y,s} = J_s \sum_{j=1}^\infty \sum_{k=1}^\infty \frac{A_{j,k}}{n_k} \left[\cos(n_k h_{2s}) - \cos(n_k h_{1s})\right] \left[\sin(m_j d_{2s}) - \sin(m_j d_{1s})\right]. \tag{31}$$

3. Computation of leakage fields on LV and HV windings

The parameters of a three-phase amorphous transformer are given in Table 1. This is also a typical problem applied to calculate the forces (F_x and F_y) in the LV and HV windings under the three-phase short-circuit condition.

Table 1. Basic parameters of the employed amorphous transformer

No.	Parameter	Value	Unit
1	No. of phases	3	
2	Frequency	50	Hz
3	Rated power	160	kVA
4	Windings connections	Delta/Wye	
5	HV/LV	22/0.4	kV
6	No. of turns of HV/LV windings	2 802/28	
7	Phase current in HV/LV windings	2.42/231	A
8	Short-circuit current in HV/LV windings	57.9/5526.3	A

The dimensions of the magnetic circuit and windings are presented in Fig. 4.
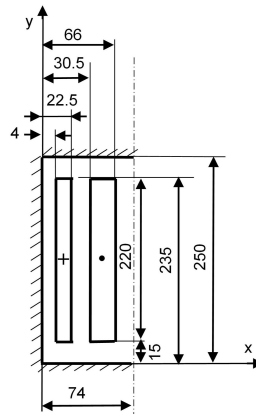
Fig. 4. Dimensions of magnetic circuit and windings of the employed transformer

In this paper, a three-phase short-circuit is applied to the amorphous transformer. Thus, the transient current is expressed [3, 5, 7]:

$$i = i' + i'' = I_n\sqrt{2}\sin(\omega t - \varphi_n) + I_n\sqrt{2}\sin\varphi_n e^{-\frac{R_n}{X_n}\omega t}, \tag{32}$$

where the current i consists of two components, i.e., the alternating and sinusoidal component i' and the aperiodic component i''. ϕ_n, R_n, and X_n are the phase angle of the short-circuit current, short-circuit resistance, and short-circuit reactance, respectively.

Based on the basic parameters of the transformer given in Table 1, the transient currents in the LV and HV windings are respectively calculated as follows:

$$i_{n\text{HV}} = i' + i'' = 57.9\sqrt{2}\sin\left(100\pi t - 1.57°\right) + 57.9\sqrt{2}\sin 90.2° e^{-\frac{114.5}{91.6}100\pi t}, \tag{33}$$

$$i_{n\text{LV}} = i' + i'' = 5526.3\sqrt{2}\sin\left(100\pi t - 1.57°\right) + 5526.3\sqrt{2}\sin 90.6° e^{-\frac{114.5}{91.6}100\pi t}. \tag{34}$$

The transient currents in Eq. (33) and Eq. (34) are pointed out in Fig. 5 and Fig. 6. It can be seen that the currents reach maximum values at the first peak of 118.7 (A) for the HV winding and 10 397 (A) for the LV winding.
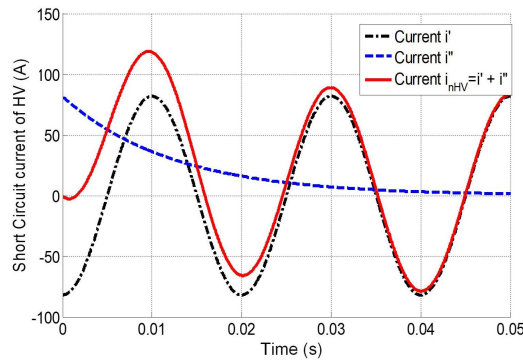
Fig. 5. Transient current in the HV winding
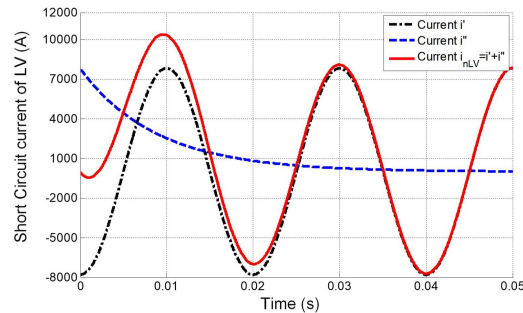
Fig. 6. Transient current in the LV winding

Based on Eq. (14), the current densities in the LV and HV windings can be respectively calculated as:

$$J_1 = J_{n\text{LV}} = \frac{W_{\text{LV}}i_{n\text{LV max}}}{a_1 b_1} = \frac{28 \times 10397}{30.5 \times 220} \times 10^6 = 43.38 \times 10^6, \tag{35}$$

$$J_2 = J_{n\text{HV}} = \frac{W_{\text{HV}}i_{n\text{HV max}}}{a_2 b_2} = \frac{2802 \times 118.7}{25.5 \times 220} \times 10^6 = 59.28 \times 10^6. \tag{36}$$

In addition, based on Eqs. (26), (27), and (28), the term of A can be determined as:

$$A = A_{1,k} + A_{j,1} + A_{j,k},$$ (37)

$$A_{1,k} = \sum_{k=1} \cos(n_k y) \frac{2\mu_0}{n_k^3 dh} \left\{ \begin{array}{l} J_1(d_{21} - d_{11})\left[\sin(n_k h_{21}) - \sin(n_k h_{11})\right] \\ +J_2(d_{22} - d_{12})\left[\sin(n_k h_{22}) - \sin(n_k h_{12})\right] \end{array} \right\},$$ (38)

$$A_{j,1} = \sum_{j=1} \cos(m_j y) \frac{2\mu_0}{m_j^3 dh} \left\{ \begin{array}{l} J_1(h_{21} - h_{11})\left[\sin(m_j d_{21}) - \sin(m_j d_{11})\right] \\ +J_2(h_{22} - h_12)\left[\sin(m_j d_{22}) - \sin(m_j d_{12})\right] \end{array} \right\},$$ (39)

$$A_{j,k} = \sum_{k=2}\sum_{j=2} \left\{ \begin{array}{c} \cos(n_k y)\cos(m_j x)\dfrac{4\mu_0}{dh}\dfrac{1}{m_j n_k\left(m_j^2 + n_k^2\right)}\times \\ \left\{ \begin{array}{l} J_1\left[\sin(m_j d_{21}) - \sin(m_j d_{11})\right]\left[\sin(n_k h_{21}) - \sin(n_k h_{11})\right] \\ +J_2\left[\sin(m_j d_{22}) - \sin(m_j d_{12})\right]\left[\sin(n_k h_{22}) - \sin(n_k h_{12})\right] \end{array} \right\} \end{array} \right\}.$$ (40)

The components of magnetic fields in the x and y axes at the boundaries of the window can be derived as:

$$B_x = \frac{\partial A}{\partial y} = \frac{\partial\left(A_{1,k} + A_{j,1} + A_{j,k}\right)}{\partial y},$$ (41)

$$B_y = -\frac{\partial A}{\partial x} = -\frac{\partial\left(A_{1,k} + A_{j,1} + A_{j,k}\right)}{\partial x}.$$ (42)

By substituting Eqs. (38), (39) and (40) into Eq. (41) and Eq. (42), the components of the magnetic field are expressed as:

$$B_x = -\sum_{k=1}\sin(n_k y)\frac{2\mu_0}{n_k^3 dh}\left\{ \begin{array}{l} J_1(d_{21} - d_{11})\left[\sin(n_k h_{21}) - \sin(n_k h_{11})\right] \\ +J_2(d_{22} - d_{12})\left[\sin(n_k h_{22}) - \sin(n_k h_{12})\right] \end{array} \right\}$$
$$-\sum_{k=2}\sum_{j=2}\left\{ \begin{array}{c} \sin(n_k y)\cos(m_j x)\dfrac{4\mu_0}{dh}\dfrac{\mu_0}{m_j n_k\left(m_j^2 + n_k^2\right)}\times \\ \left\{ \begin{array}{l} J_1\left[\sin(m_j d_{21}) - \sin(m_j d_{11})\right]\left[\sin(n_k h_{21}) - \sin(n_k h_{11})\right] \\ +J_2\left[\sin(m_j d_{22}) - \sin(m_j d_{12})\right]\left[\sin(n_k h_{22}) - \sin(n_k h_{12})\right] \end{array} \right\} \end{array} \right\},$$ (43)

$$B_y = \sum_{j=1}\sin(m_j y)\frac{2\mu_0}{m_j^3 dh}\left\{ \begin{array}{l} J_1(h_{21} - h_{11})\left[\sin(m_j d_{21}) - \sin(m_j d_{11})\right] \\ +J_2(h_{22} - h_{12})\left[\sin(m_j d_{22}) - \sin(m_j d_{12})\right] \end{array} \right\}$$
$$+\sum_{k=2}\sum_{j=2}\left\{ \begin{array}{c} \cos(n_k y)\sin(m_j x)\dfrac{4\mu_0}{dh}\dfrac{\mu_0}{m_j n_k\left(m_j^2 + n_k^2\right)}\times \\ \left\{ \begin{array}{l} J_1\left[\sin(m_j d_{21}) - \sin(m_j d_{11})\right]\left[\sin(n_k h_{21}) - \sin(n_k h_{11})\right] \\ +J_2\left[\sin(m_j d_{22}) - \sin(m_j d_{12})\right]\left[\sin(n_k h_{22}) - \sin(n_k h_{12})\right] \end{array} \right\} \end{array} \right\}.$$ (44)

For $j, k = \overline{1, 30}$, the distribution of magnetic vector potential A can be presented in Fig. 7.

Similarly, the components of the magnetic field in the LV and HV windings are depicted in Fig. 8 and Fig. 9, respectively.
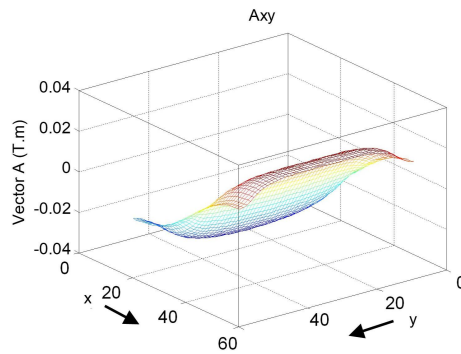
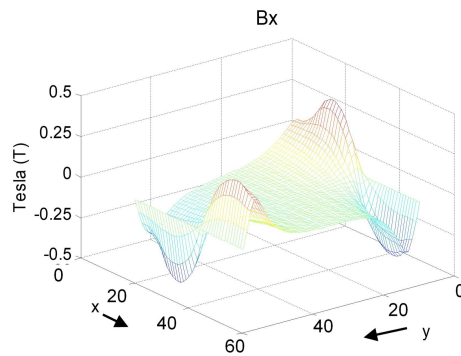Fig. 7. Distribution of magnetic vector potential A by using the proposed model

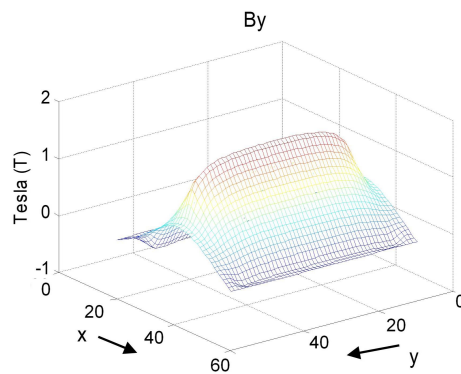Fig. 8. Radial component of magnetic field (B_x) by using the proposed model

Fig. 9. Axial component of magnetic field (B_y) by using the proposed model

As shown in Fig. 8, the distribution of the term of B_x along the y-axis is concentrated on the two ends of the windings, for $B_{x\,\text{max}} = 0.43$ T. In the middle of the winding, this field becomes smaller, because the magnetic field is bent at the two ends of the winding. In the x-axis, the

direction is reversed because the currents in the two windings are in opposite directions. In Fig. 9, the distribution of the term of B_y along the y-axis becomes small at the two ends of the winding and large in the middle of the winding. On the other hand, in the x-axis, the B_x gradually increases and gets the maximum value at the middle of the winding, for $B_{y\,max} = 1.76$ T.

Based on Eq. (30) and Eq. (31), F_x and F_y in the LV and HV windings are presented in Fig. 10 and Fig. 11, respectively.
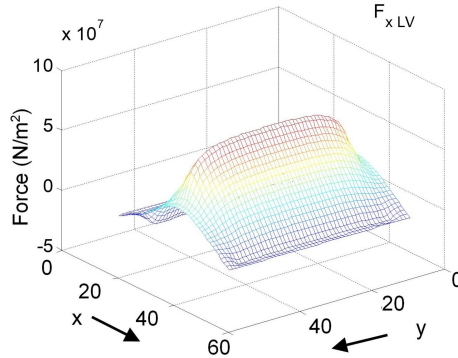
Fig. 10. Distribution of $F_{x\text{LV}}$ in the LV winding by using the proposed model
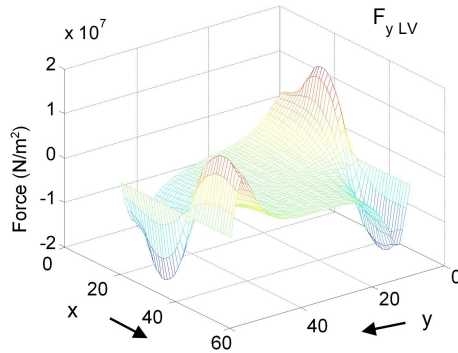
Fig. 11. Distribution of $F_{y\text{LV}}$ in the LH winding by using the proposed model

In Fig. 10, along the y-axis (height of winding), the LV winding is pushed inwards by F_x. The distribution of the magnetic field gradually decreases to the two ends of the winding and gets the maximum value at the middle of the winding, with $F_{x\text{LV}\,max} = 7.419 \times 10^7$ (N/m^2). In Fig. 11, the distribution of F_y is concentrated at the two ends of the winding with $F_{y\text{LV}\,max} = 1.862 \times 10^7$ (N/m^2) and becomes a zero in the middle of the winding.

For the HV winding, F_x and F_y in the windings are illustrated in Fig. 12, and Fig. 13, respectively.

In Fig. 12, it can be seen that along the y-axis, due to F_x, the HV winding is pushed away from the LV winding. The distribution of the magnetic field gradually decreases to the two ends of the
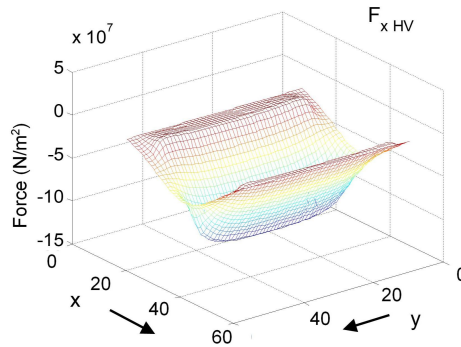
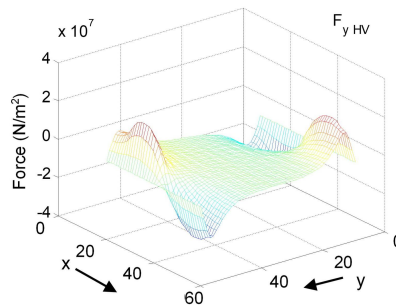Fig. 12. Radial force (F_{xHV}) in the HV winding by using the proposed model

Fig. 13. Axial force (F_{yHV}) in the HV winding by using the proposed model

winding and gets the maximum value at the middle of the winding, for $F_{xHV\,max} = 0.552 \times 10^7$ (N/m^2). In Fig. 13, the distribution of F_y is concentrated at the two ends of the winding, for $F_{yHV\,max} = 2.553 \times 10^7$ (N/m^2) and also becomes a zero in the middle of the winding.

4. Numerical test by using FEM

In order to compare with the proposed model, in this section, F_x and F_y are simulated by using the FEM via ANSYS MAXWELL software [23]. Based on the parameters of the amorphous core transformer already given in Table 1, the distribution of the magnetic field is pointed out in Fig. 14. In this figure, the x-axis and y-axis are the width and the height of the window.

The distributions of F_x and F_y in the LV and HV windings are shown in figures (from Fig. 15 to Fig. 17).

In Fig. 15, the distribution of F_x in the LV winding has the smallest value at the two ends of the winding. This force increases in the middle of the winding and gets the maximum value at the middle of the winding, for $F_{xLV\,max} = 7.275 \times 10^7$ (N/m^2). In Fig. 17, the distribution of F_x in the HV winding is similar to F_x in the LV winding, but it is in the opposite direction. The maximum value is at the middle of the winding, for $F_{xHV\,max} = 0.563 \times 10^7$ (N/m^2).
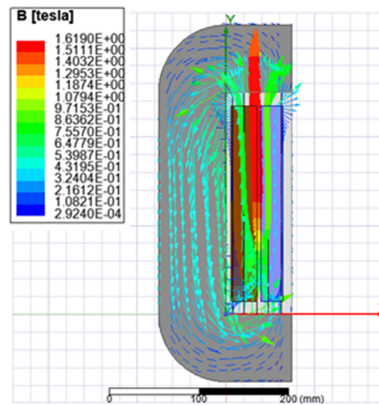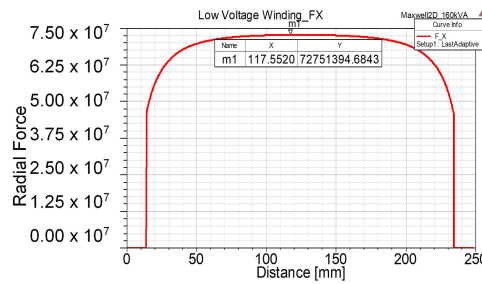
Fig. 14. Distribution of magnetic field by using FEM

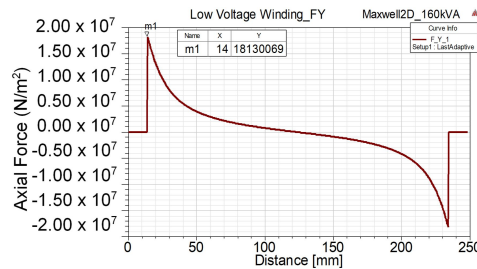Fig. 15. Distribution of $F_{x\text{LV}}$ in the LV winding by using FEM

Fig. 16. Distribution of $F_{y\text{LV}}$ in the LV winding by using FEM

In the direction of the current action, due to this force, the HV winding is pushed into the magnetic core (positive direction), and far away of the magnetic core (negative direction) for the HV winding. The distributions of F_x in the LV and HV windings are shown in Fig. 16 and Fig. 18. The maximum values of these forces at the two ends of each winding are defined as $F_{y\text{LV max}} = \pm 1.813 \times 10^7$ (N/m^2) and $F_{y\text{HV max}} = \pm 2.390 \times 10^7$ (N/m^2). These forces become zero in the middle of the windings.
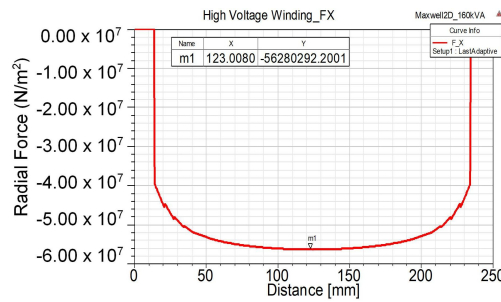
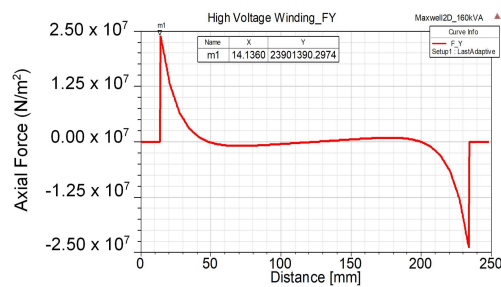Fig. 17. Distribution of $F_{x\text{HV}}$ in the HV winding by using FEM

Fig. 18. Distribution of $F_{y\text{HV}}$ in the HV winding by using FEM

Finally, the comparison of the obtained results between the two methods is presented in figures (from Fig. 19 to Fig. 22).
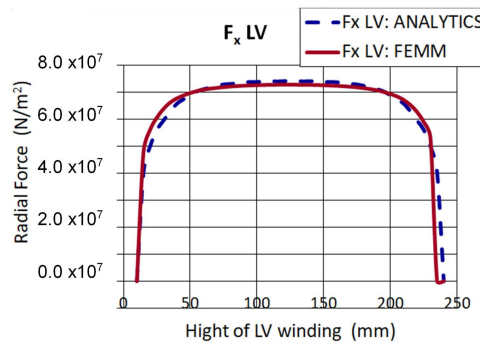

Fig. 19. Distributions of $F_{x\text{LV}}$ in the LV winding by using the proposed
model and FEM

It can be seen that the obtained results from the analytic/proposed method are checked to be close to those of by using the FEM. However, there are still differences in the forces between the two methods given in Table 2. It should be noted that the winding is acted by the $F_{x\max} = 7.149 \times 10^7$ (N/m^2), this makes the winding will be bent, compressed, and destroyed.
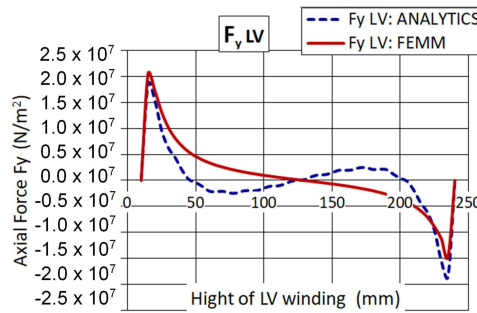
Fig. 20. Distributions of $F_{y\text{LV}}$ in the LV winding by using the proposed
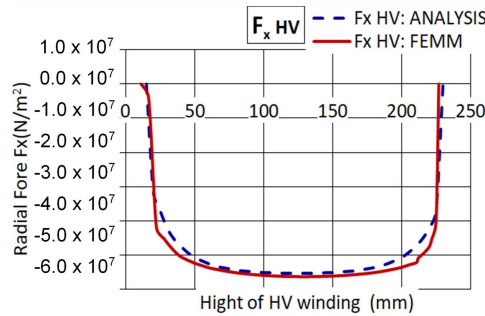model and FEM

Fig. 21. Distributions of $F_{x\text{HV}}$ in the HV winding by using the proposed
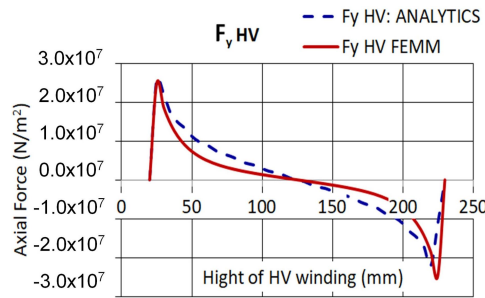model and FEM

Fig. 22. Distributions of $F_{y\text{HV}}$ in the HV winding by using the proposed
model and FEM

If the winding is considered a solid object, in which the allowable stress of copper is $\sigma_{\text{allow}} = 5.0 \times 10^7$ (N/m^2) [12]. Hence, when a short circuit occurs with the maximum current, the maximum stress of the winding will exceed over the allowable limit. On the other hand, if the short circuit occurs in a few seconds, the windings will be bent or destroyed.

Table 2. Comparative results of F_x and F_y with the two different methods

Winding	$F_{\max} \times 10^7$ (N/m^2)	The proposed model	FEM	Error (%)
LV	Radial force ($F_{x\mathrm{LV}\,\max}$)	7.419	7.275	1.9
	Axial force ($F_{y\mathrm{LV}\,\max}$)	±1.862	±1.813	2.6
HV	Radial force ($F_{x\mathrm{LV}\,\max}$)	−0.552	−0.563	2.0
	Axial force ($F_{y\mathrm{LV}\,\max}$)	±2.553	±2.390	6.3

5. Conclusions

In this paper, an analytic method has been successfully developed to calculate the leakage magnetic fields in the window of the amorphous core transformer. The vector magnetic potential formulations are then established in the form of the Laplace–Poisson equation. Based on the development, F_x and F_y in the LV and HV windings of the amorphous transformer are investigated and analyzed. The distributions of the magnetic vector potential, leakage magnetic fields in the window, and F_x and F_y in the LV and HV windings of an amorphous transformer of 160 kVA–22/0.4 kV under a three-phase short-circuit condition have been presented with the proposed model. The obtained results have been thus compared with those from the FEM to verify the validation of the proposed model.

Acknowledgements

References

[1] Harry W.N., Hasegawa R., Albert L., Lowdermilk L.A., *Amorphous Alloy Core Distribution Transformers*, Proceedings of the IEEE, vol. 79, no. 11, pp. 1608–1623 (1991), DOI: 10.1109/5.118984.

[2] Steinmetz T., Cranganu-Cretu B., Smajic J., *Investigations of no-load and load losses in amorphous core dry-type transformers*, The XIX International Conference on Electrical Machines – ICEM 2010, pp. 1–6 (2010), DOI: 10.1109/ICELMACH.2010.5608162.

[3] De Azevedo A.C., Delaiba A.C., De Oliveira J.C., Carvalho B.C., Herivelto de Souza Bronzeado, *Transformer mechanical stress caused by external short-circuit: a time domain approach*, Presented at the International Conference on Power Systems Transients (IPST'07) in Lyon, France (2007), https://www.scribd.com/document/285008792/2007.

[4] Bahmani M.A., *Core Loss Calculation in Amorphous High Frequency High Power Transformers with Different Topologies*, Master of Science Thesis in Electric Power Engineering – Chalmers University of Technology Sweden, pp. 1–65 (2011), https://odr.chalmers.se/handle/20.500.12380/142830.

[5] Ahn H.M., Oh Y.H., Kim J.K., Song J.S., Hahn S.C., *Experimental Verification and Finite Element Analysis of Short-Circuit Electromagnetic Force for Dry-Type Transformer*, IEEE Transactions on Magnetics, vol. 48, no. 2, pp. 819–822 (2012), DOI: 10.1109/TMAG.2011.2174212.

[6] Marcel Dekler, *Transformer Engineering Design and Practice – Chapter 6: Short Circuit Stresses and Strength*, ISBN: 0-8247-5653-3, pp. 231–275 (2000).

[7] Hyun Mo Ahn, Byuk-jin Lee, Cheri-jin Kim, Heung-kyo Shin, Sung-chin Hahn, *Finite Element Modeling of Power Transformer for Short-circuit Electromagnetic Force Analysis*, International Conference on Electrical Machines and Systems, INSPEC Accession Number: 13247968, vol. 15, pp. 5–8 (2012).

[8] Zakrzewski K., Tomczuk B., Koteras D., *Simulation of forces and 3-d field arising during power autotransformer fault due to electric arc in HV winding*, IEEE Transactions on Magnetics, vol. 38, no. 2, pp. 1153–1156 (2002), DOI: 10.1109/20.996295.

[9] Allahbakhsi M., Abbaszadeh K., Akbari A., *Effect of asymmetrical dimensions in short circuit forces of power transformers*, IEEE International Conference on Electrical Machines and Systems, vol. 3, no. 1, pp. 1746–1749 (2005), DOI: 10.1109/ICEMS.2005.202858.

[10] Feyzi M.R., Sabahi M., *Finite element analyses of short circuit forces in power transformers with asymmetric conditions*, 2008 IEEE International Symposium on Industrial Electronics, no. 1, pp. 576–581 (2008), DOI: 10.1109/ISIE.2008.4677272.

[11] Sinha A., Kaur S., *Analysis of short circuit electromagnetic forces in transformer with asymmetrically placed windings using Finite Element Method*, 2016 Second International Innovative Applications of Computational Intelligence on Power, Energy and Controls with their Impact on Humanity (CIPECH), pp. 101–105 (2009), DOI: 10.1109/CIPECH.2016.7918746.

[12] Sharifian M.B.B., Esmaeilzadeh R., Farrokhifar M., Faiz J., Ghadimi M., Ahrabian G., *Computation of a Single-phase Shell-Type Transformer Windings Forces Caused by Inrush and Short-circuit Currents*, Journal of Computer Science, vol. 4, no. 1, pp. 51–58 (2008), DOI: 10.3844/jcssp.2008.51.58.

[13] Kashtiban A.M., Vahedi A., Halvaei A., *Investigation of Winding Type E ffect on Leakage Flux of Single Phase Shell Type Transformer Using FEM*, International Conference on Electrical Machines and Systems, pp. 1755–1758 (2005), DOI: 10.1109/ICEMS.2005.202860.

[14] Zakrzewski K., Tomczuk B., Koteras D., *Amorphous modular transformers and their 3D magnetic fields calculation with FEM*, The International Journal for Computation and Mathematics in Electrical and Electronic Engineering, vol. 28, no. 3, pp. 583–592 (2009), DOI: 10.1108/03321640910950034.

[15] Zhang H., Yang B., Xu W., Wang S., Wang G., Huangfu Y., Zhang J., *Dynamic Deformation Analysis of Power Transformer Windings in Short-Circuit Fault by FEM*, IEEE Transactions on Applied Superconductivity, vol 24, no. 3 (2013), DOI: 10.1109/TASC.2013.2285335.

[16] Ahmad A., Javed I., Nazar W., Asim Mukhtar M., *Short Circuit Stress Analysis Using FEM in Power Transformer on H-V Winding Displaced Vertically and Horizontally*, International Journal of Emerging Technology and Advanced Engineering, vol. 57, no. 1 (2018), DOI: 10.1016/j.aej.2016.10.006.

[17] Kumbhar G.B., Kulkarni S.V., *Analysis of Short-Circuit Performance of Split – Winding Transformer Using Coupled Field-Circuit Approach*, IEEE Transactions on Power Delivery, vol. 22, no. 2, pp. 936–943 (2007), DOI: 10.1109/TPWRD.2007.893442.

[18] Ahmad A., Javed I., Nazar W., Mukhtar M.A, *Short Circuit Stress Analysis Using FEM in Power Transformer on H-V Winding Displaced Vertically and Horizontally*, Alexandria Engineering Journal, vol. 57, iss. 1, pp. 147–157 (2018), DOI: 10.1016/j.aej.2016.10.006.

[19] Wang Y., Zhao X., Han J., Li H., Guan Y., Bao Q., Xiao L., Lin L., Xu X., Song N., Zhang F., *Development of a 630 kVA Three-Phase HTS Transformer with Amorphous Alloy Cores*, IEEE Transactions on Applied Superconductivity, vol. 17, no. 2, pp. 2051–2054 (2007), DOI: 10.1109/TASC.2007.898162.

[20] Zhong H., Niu W., Lin T., Han D., Zhang G., *The Analysis of Short-Circuit Withstanding Ability for A 800KVA/10KV Shell-Form Power Transformer with Amorphous Alloy Cores*, 2012 IEEE International Conference on Electricity Distribution (CICED), no. 2161–7481, pp. 1–5 (2012), DOI: 10.1109/CICED.2012.6508689.

[21] Tomczuk B., Zakrzewski K., Koteras D., *Magnetic Field and Short-Circuit Reactance Calculation of the 3-phase Transformer with Symmetrical Amorphous Core*, Book – Computer Engineering in Applied Electromagnetism, 11th, pp. 227–230 (2005), DOI: 10.1007/1-4020-3169-6_39.

[22] Mouhamad M., Elleau C., Mazaleyrat F., Guillaume C., Jarry B., *Short-Circuit Withstand Tests of Metglas 2605SA1-Based*, IEEE Transactions on Magnetics, vol. 47, no. 10, pp. 4489–4492 (2011), DOI: 10.1109/TMAG.2011.2155632.

[23] ANSYS Inc., *ANSYS Maxwell 3D V19*, ansysinfo@ansys.com, vol. 19, no. REV5.0, pp. 1–1011 (2016).